Fault-induced polytypism in (Cr, Fe)$_2$B

I. Goldfarb [a] , W. D. Kaplan [b] , S. Ariely [c] & M. Bamberger [d]

[a] Department of Materials, University of Oxford, Ox1 3Ph,
England

[b] Max-Planck-Institut fur Metallforschung, Institut für
Werkstoffwissenschaft, Seestrasse 92, D-70174, Stuttgart,
Germany

[c] Israel Electric Company, Haifa, Israel

[d] Department of Materials Engineering, Technion—Israel Institute
of Technology, Haifa, 32000, Israel
Version of record first published: 27 Sep 2006.

PLEASE SCROLL DOWN FOR ARTICLE

Fault-induced polytypism in (Cr, Fe)₂B

By I. GOLDFARB

Department of Materials, University of Oxford OX1 3PH, England

W. D. KAPLAN

Max-Planck-Institut für Metallforschung, Institut für Werkstoffwissenschaft, Seestrasse 92, D-70174, Stuttgart, Germany

S. ARIELY

Israel Electric Company, Haifa, Israel

and M. BAMBERGER

Department of Materials Engineering, Technion—Israel Institute of Technology, Haifa 32000, Israel

ABSTRACT

The microstructures of chromium and iron borides formed during laser surface alloying of AISI 1045 steel with CrB were examined by transmission electron microscopy combined with selected-area electron diffraction and X-ray-dispersive spectroscopy. It was found that the heavily faulted $(Cr, Fe)_2B$ phase contains a microsyntactic existence of several polytypes, including one-dimensionally disordered structures as well as fully developed lamellae of ordered polytypes, similar to those found in SiC. Classification of $(Cr, Fe)_2B$ as a polytype was made for the first time and is described in detail. It was found that in this case polytypism originates from the $(Fe, Cr)_2B \rightarrow (Cr, Fe)_2B$ transformation in the solid state by the introduction of stacking faults in the $(Fe, Cr)_2B$ phase, owing to a close similarity between the structures of both phases. This transformation is directly responsible for the mentioned microsyntaxy and was experimentally observed through transmission electron microscopy.

§ 1. INTRODUCTION

The introduction of boron and subsequent formation of Fe–B compounds can improve the hardness and wear resistance of steels. Traditional methods of boronizing involve heating steels in the presence of boron powders to high temperatures for relatively long periods of time (Graf von Matuschka 1977). However, such alloying techniques can also lead to significant grain growth and thus a reduction in strength of the bulk material. Laser surface alloying can improve surface properties while leaving the bulk unaffected. Recently, laser surface alloying of steel and iron with CrB_2 particles was conducted (Shafirstien, Bamberger, Langohr and Maisenhalder 1991, Bamberger *et al.* 1991). A variety of phases was found by X-ray diffraction (XRD) in the reacted surface layer, including residual unmelted CrB_2 and Fe_2B which formed during solidification on iron substrates, and martensite, γ-Fe, Cr_3C_2 and Fe_3B on steel substrates. It was difficult to explain the existence of all these phases on the basis of scanning electron microscopy (SEM) examination only.

In order to overcome this difficulty the microstructure resulting from laser alloying must be examined by a more powerful method, such as transmission electron microscopy (TEM). TEM is a versatile analytical method which can yield visual, crystallographic and compositional information from regions of interest on a *microscale*. Phase formation and transformations can be clearly observed by TEM. However, there are relatively very few papers on microstructural investigations of laser-alloyed surfaces by this method (Hornbogen and Staniek 1988), although there are several TEM studies on boride-steel alloys prepared by other processes (García-Bórquez and Kesternich 1985, Yijian and Jian 1991, Wang, Zhu and Haasen 1991, Kotani, Ishimasa and Oki 1993). Because of the lack of microstructural examinations the nature of laser-formed phases and mechanisms of transformations and kinetics are not known.

The goal of this work was to identify the phases which formed in CrB laser-alloyed steel by detailed TEM examination of the resulting microstructures.

§ 2. Experimental

Specimens of AISI 1045 steel 10 mm thick were mechanically polished before alloying by a Rofin Sinar CO_2 2500 laser with a 1750 W output, a 2 mm beam diameter, $0 \cdot 01 \, m \, s^{-1}$ scanning velocity and 50% overlap between each pass of the laser. CrB powder (particle size, 100–150 μm) was fed into the molten bath in the vicinity of the cross-point of the laser beam with the substrate. A Plasma Technik powder feed apparatus was used with Ar which served both as a carrier and an oxidation-protective gas.

A JEOL-840 scanning electron microscope equipped with a standard Link energy-dispersive spectrometer was used for examination of the surface morphology and for quantitative microanalysis. XRD spectra were measured in Bragg–Brentano parafocusing geometry using an automated Phillips diffractometer, equipped with a bent graphite monocromator and a Cu radiation tube. XRD spectra were routinely obtained in a step mode with step size $\Delta \, (2\Theta) = 0 \cdot 07°$ and exposure per step of 40 s. Microstructural investigations were conducted on a JEOL 2000 FX scanning transmission electron microscope combined with selected-area electron diffraction (SAED) and a Link energy-dispersive spectrometer for elemental microanalysis in scanning transmission electron microscopy mode. Pure sapphire crystals were used to calibrate the magnification. Microdensitometry as well as fast Fourier transforms (FFTs) were achieved by scanning negatives on a 300 dots-per-inch scanner and by sequential image analysis using the computer software Digital Micrograph, supplied by Gatan. Microdensitometry was applied to the zero-and the first-order rows of the SAED patterns.

§ 3. Results

A typical secondary-electron SEM image of a CrB laser-alloyed steel specimen is shown in fig. 1. It consists of large curve-shaped dark particles about 10–15 μm in size surrounded by thinner and brighter columnar grains. In between the columnar grains a fine microstructure is observed which has a bright contrast. Energy-dispersive spectroscopy (EDS) line scans (not shown here) show a high and constant concentration of Cr across the curve-shaped particles, which decreases abruptly at the boundary between the particles and the columnar grains to approximately half of the original intensity. At the boundary between the columnar grains and the underlying steel matrix there is a further abrupt decrease in Cr concentration. The Fe intensity distribution exhibits the opposite behaviour, that is no Fe inside the curve-shaped particle, a sharp

Fig. 1

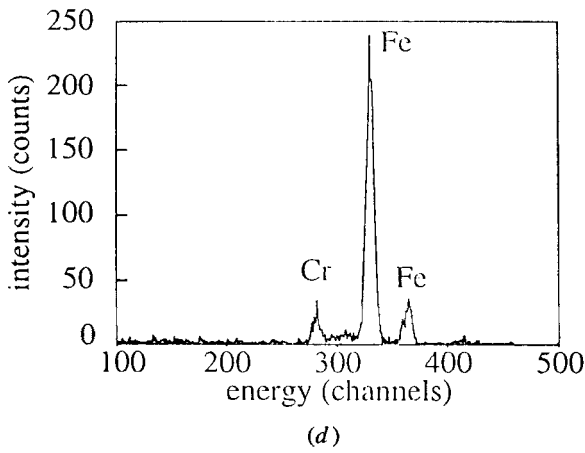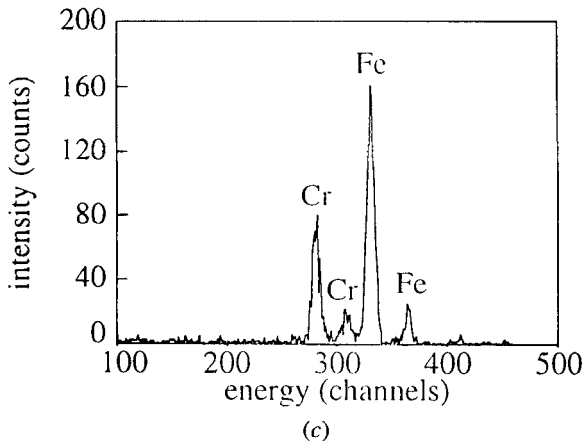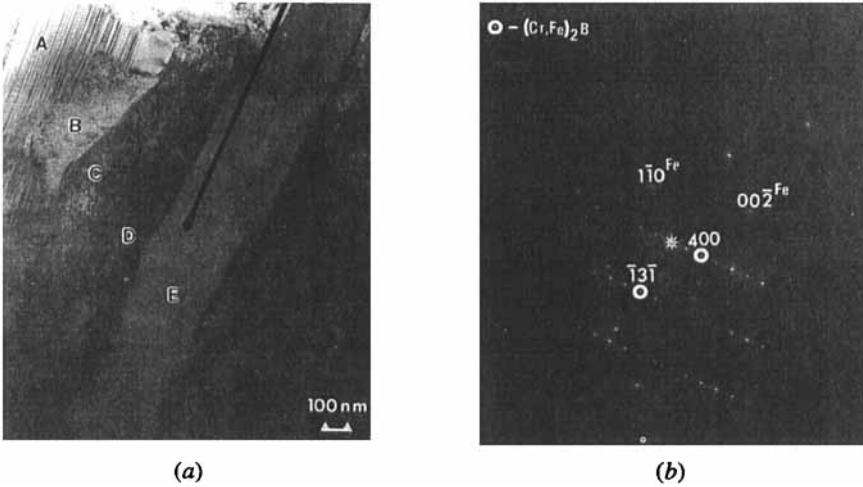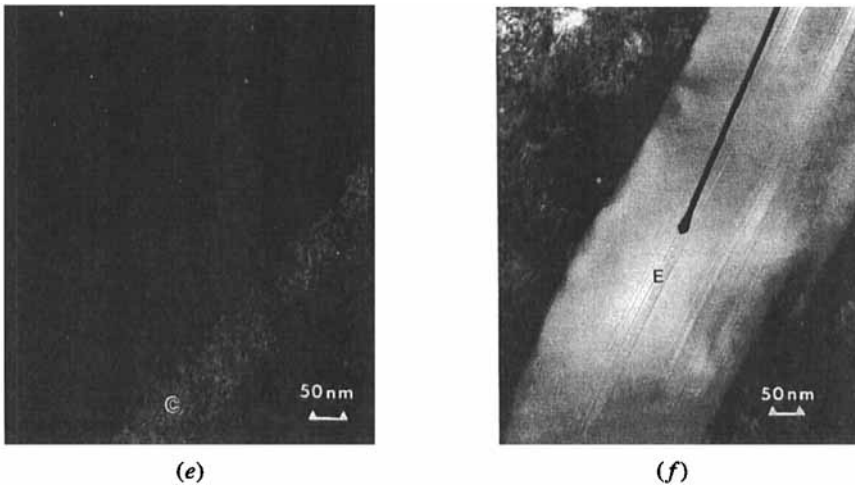Typical secondary-electron SEM image of the AISI 1045 steel laser alloyed with CrB.

Fig. 2
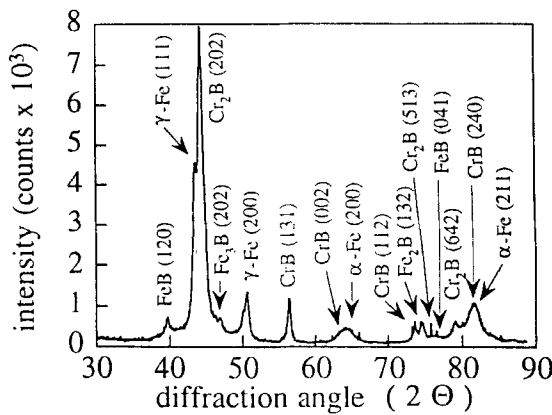
Typical XRD pattern of the AISI 1045 steel laser alloyed with CrB.

increase at the boundary between the particle and the columnar grains, and a further increase at the boundary with the matrix. A typical XRD pattern is shown in fig. 2 and indicates the variety of phases formed, such as iron and chromium borides in addition to α- and γ-Fe originating from the substrate. It should be stated that there is some uncertainty involved in phase identification by XRD due to the similarity of interatomic spacings of various Cr and Fe borides and carbides. Yet the phases designated in fig. 2, namely CrB, $(Fe, Cr)_2B$, $(Fe, Cr)B$, $(Cr, Fe)_2B$, α- and γ-Fe, and $(Fe, Cr)_3B$ are the most probable, as explained in the next sections.

Figure 3 (a) shows a typical bright-field (BF) low-magnification TEM image of the microstructure and fig. 3 (b) presents the SAED pattern from the same area, which consists of two superimposed patterns. Energy-dispersive spectra from areas designated A, B, C, D and E are given in figs. 3 (c) and (d). The spectra from A and E were identical, showing Fe and Cr, while spectra from B, C and D were identical and indicated only negligible Cr concentration. Both SAED patterns observed in fig. 3 (b) were identified as α-Fe [110] and $(Cr, Fe)_2B$ [01$\bar{3}$] which exhibited streaking in the [100] direction. Dark-field (DF) images using α-Fe and $(Cr, Fe)_2B$ reflections are shown in

I. Goldfarb *et al.*

Fig. 3

(a)

$\bigcirc - (Cr,Fe)_2B$

$1\bar{1}0^{Fe}$ $00\bar{2}^{Fe}$

400

$\bar{1}3\bar{1}$

(b)

(c)

(d)

(e) (f)

Typical microstructure of the AISI 1045 steel laser alloyed with CrB as seen by TEM: (a) BF image indicating various regions of interest differing in contrast; (b) SAED pattern consisting of the α-(Fe, Cr) [110] and the $(Cr, Fe)_2B$ [01$\bar{3}$] (circled) reflections (note the mutually perpendicular directions of the streaking and the fault planes in A and E); (c) EDS spectrum characteristic of the faulted $(Cr, Fe)_2B$ grains designated A and E; (d) EDS spectrum characteristic of the α-(Fe, Cr) grains designated B–D; (e) DF image obtained using the α-(Fe, Cr) reflections (region C); (f) DF image obtained using the $(Cr, Fe)_2B$ reflections (region E).

Fig. 4

(a) (b)
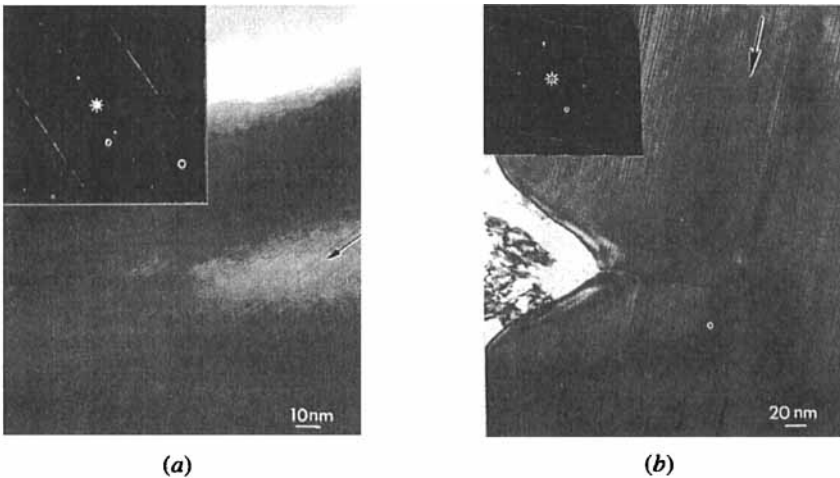
Additional $(Cr, Fe)_2B$ grains (the respective SAED patterns are given in the insets): (a) a faulted grain exhibiting a larger degree of spottiness in comparison with (b); (b) a faulted grain exhibiting an intense diffuse streaking in the [100] direction.

Fig. 5
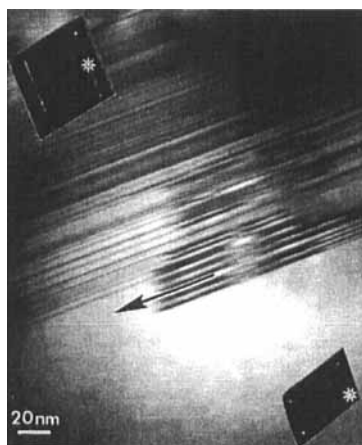
A partially faulted grain. The SAED patterns from both the faulted and the unfaulted portions are shown in the respective insets.

figs. 3 (*e*) and (*f*) respectively. It can be concluded that this region consists of $(Cr, Fe)_2B$ grains surrounded by α-Fe. A dense configuration of stacking faults in $(Cr, Fe)_2B$ grains (A and E in figs. 3 (*a*) and (f)) could be responsible for the streaking of the diffraction spots in fig. 3 (*b*), since these faults lie on {100} crystallographic planes which are exactly perpendicular to the direction of streaking.

In order to investigate this point further, two additional faulted grains were brought into exact Bragg conditions, and their BF images are shown in figs. 4 (*a*) and (*b*) (their SAED patterns are present in the respective insets). It should be noted that, although all the faulted grains are oriented approximately the same, there is a slight misorientation between them. Misorientation can be observed as a non-straight image of fault fringes (area A in fig. 3 (*a*)), relative to the straight fringes which are 'edge on' to the electron beam (area E in fig. 3 (*a*)). In addition, many grains were found to be partially faulted, as shown in fig. 5. SAED patterns from the faulted region and from the unfaulted region are shown in the inset.

§ 4. DISCUSSION

4.1. *Correlation between the images and the diffraction patterns*

Although the phenomenon of a $(Cr, Fe)_2B$ faulted structure was observed in several investigations (Garcí-Bórquez and Kesternich 1985, Kesternich and Meertense 1986, Yijian and Jian 1991, Kotani *et al.* 1993), only two studies have offered explanations (Yijian and Jian 1991, Kotani *et al.* 1993). In both papers (Yijian and Jian 1991, Kotani *et al.* 1993) a detailed microstructural analysis was conducted, but in our opinion this microstructure is more complex than follows from their explanations, and a more detailed explanation than offered by these workers is required, one that extends beyond simple faulting or/and twinning. The current work reveals that $(Cr, Fe)_2B$ has all the characteristics of a new polytype.

Figure 6 (*a*) shows a high-magnification phase contrast image of the grain from fig. 4 (*a*). The corresponding magnified SAED, superimposed with its densitometry and a computer-simulated pattern is shown in fig. 6 (*b*). Figures 7 (*a*) and (*b*) show the same for the grain in fig. 4 (*b*). Two images (figs. 6 (*a*) and 7 (*a*)) are magnified to the

Fig. 6
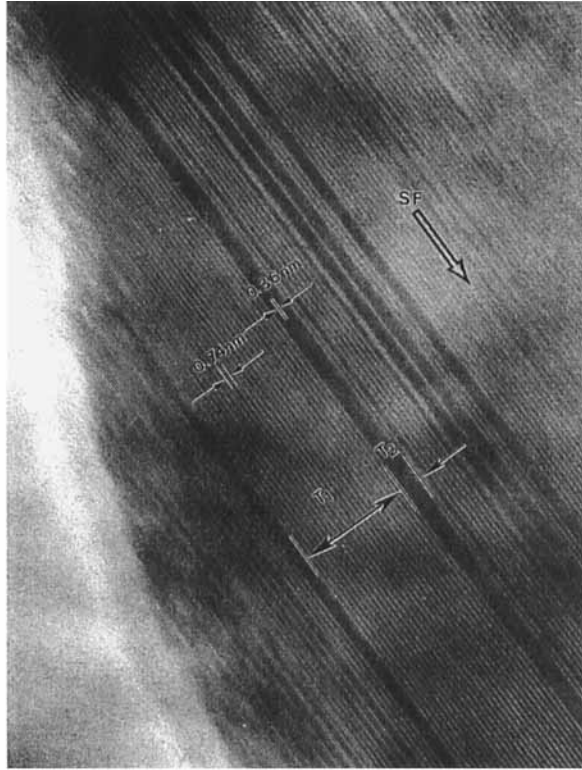
(a)
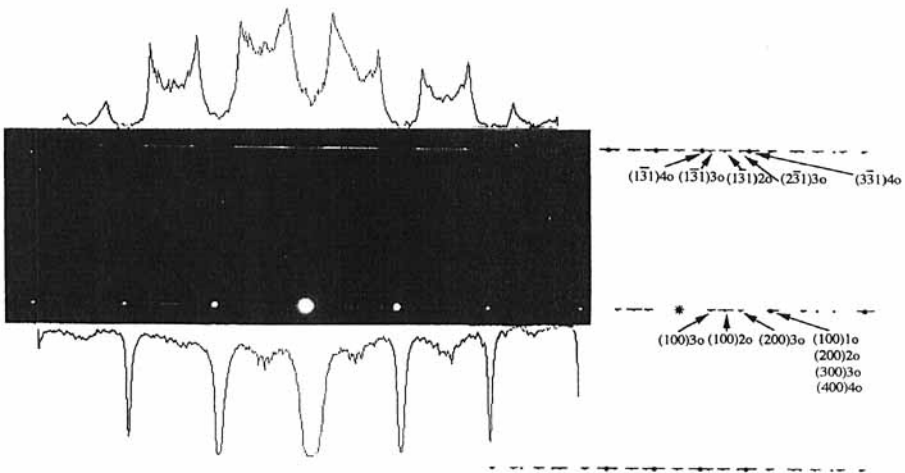
(b)

High-magnification analysis of the grains shown in fig. 4. (a) Phase contrast image of a grain in fig. 4 (a). T$_1$ and T$_2$ are the thicknesses of the 2o and the 1o lamellae respectively. One 1o layer is by definition a stacking fault SF. (b) The magnified (Cr, Fe)$_2$B [01$\bar{3}$] SAED pattern combined with the densitometric scans of the zero- and the first-order diffraction rows. The computer simulation is given on the right-hand side. The contributions from polytypes of various spacings are indicated.

I. Goldfarb *et al.*

Fig. 7

(a)

(b)
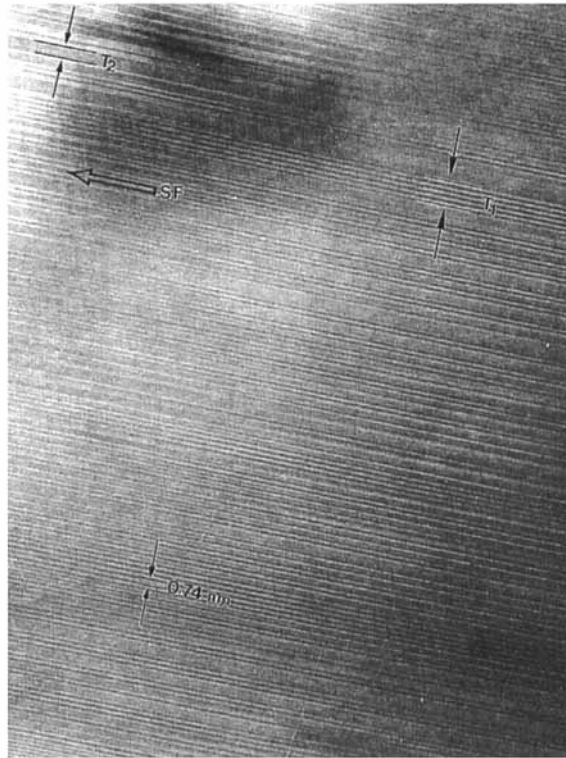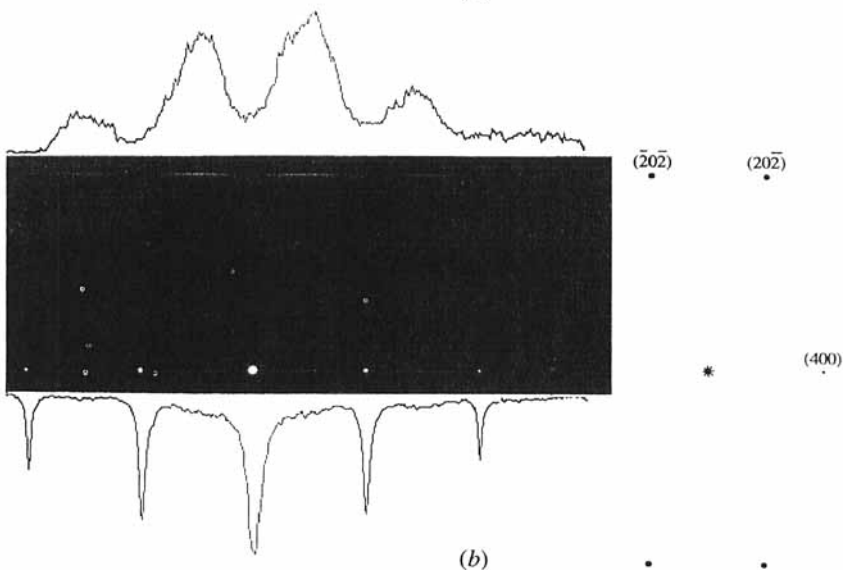
High-magnification analysis of the grains shown in fig. 4. (*a*) Phase contrast image of a grain in fig. 4 (*b*). T_1 and T_2 are the thicknesses of the 2o and the 1o lamellae respectively. One 1o layer is by definition a stacking fault SF. (*b*) The magnified $(Cr, Fe)_2B$ [010] SAED pattern combined with the densitometric scans of the zero- and the first-order diffraction rows. The computer simulation is given on the right-hand side. The contributions from polytypes of various spacings are indicated.

Fig. 8

Cr_2B (001) Fe_2B (001) Cr_2B (100)

(a)   (b)   (c)

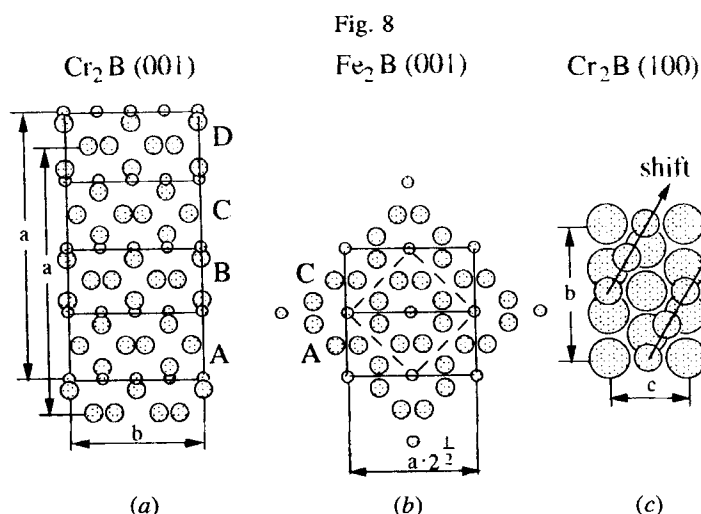Various crystallographic sections of the $(Cr, Fe)_2B$ and the $(Fe, Cr)_2B$ structures: The larger atoms are Cr and Fe and the smaller atoms are B. The heights of the A, B, C and D basic units are about 0·36 nm in both the $(Cr, Fe)_2B$ and the $(Fe, Cr)_2B$ structures; (a) the 'ball-and-stick' representation of the $(Cr, Fe)_2B$ (001) section; (b) the 'ball-and-stick' representation of the $(Fe, Cr)_2B$ (100) section; (c) the 'fill-space' representation of the $(Cr, Fe)_2B$ (100) section (the arrowed B atoms are the lowest B atoms in the A basic unit shown in (a)).

same extent and both exhibit fringes with various spacings; the smallest spacing between the fringes corresponds to about 0·36 nm and the others are integral multiples of this spacing, that is $(0·36 nm)_n$. The images differ considerably in their appearance. Figure 7 (a) resembles the one-dimensionally disordered structures of SiC (Shinozaki and Kinsman 1977, Ogbuji, Mitchell and Heuer 1981a, Carduner *et al.* 1990), while fig. 6 (a) has the characteristic appearance of a more ordered polytype with preferentially developed lamellae of one type; $n = 2$ (Ogbuji *et al.* 1981a). This difference is confirmed by their respective SAED patterns; microdensitometry of the SAED which belongs to the disordered stacking showing almost featureless streaks (fig. 7 (b)), while in fig. 6 (b) some individual spots can be observed, resolved by microdensitometry.

The structure of Cr_2B (*Fddd*; oF48; Mn_4B type) is shown in fig. 8 (a) in the [010] direction. If this structure is regarded as a layered structure, then the measured spacing of 0·36 nm exactly matches a quarter of the unit cell in the [100] direction. The quarter-unit cell, which is taken as a 'basic unit' of the structure, is analogous to the spacing of two adjacent SiC double layers with Si and C in tetrahedral coordination (Verma and Krishna 1966). Three important conclusions follow from observation of fig. 8 (a).

(a) From a crystallographic standpoint it is logical to assume that this a/4 unit should be defined between B atoms since they can be shifted on the close-packed Cr atoms, presumably in the ⟨110⟩ directions, creating stacking faults as shown in fig. 8 (c).

(b) Contrary to SiC, such a basic unit does not preserve the Cr_2B stoichiometry.

(c) The Cr_2B cell can be described as a stacking of four adjacent basic units A. B, C and D. For convenience we shall introduce a new notation for the basic

orthorhombic unit ($a = 0.37$ nm, $b = 0.74$ nm and $c = 0.43$ nm) following Ramsdell notation 1o (where o means orthorhombic) (Verma and Krishna 1966). Therefore the conventional Cr_2B unit cell shall be designated as 4o. To describe the stacking sequence it is also convenient to use Zhdanov notation (Verma and Krishna 1966). The undisturbed periodicity can be written as ABCD|ABCD|.... When a stacking fault is introduced at every fifth layer, the stacking sequence can be described as ABCD|BCDA|CDAB|DABC|..., or (4444) in Zhdanov's notation. If a stacking fault is introduced at every fourth layer, the stacking sequence is ABC|ABC|..., which is similar to a close-packed sequence in f.c.c. crystals. If the stacking is disturbed at every third layer, the resulting sequence will be AB|DA|CD|BC|AB|..., or (2222). It is important to note that a stacking disorder at every second layer produces stacking sequences similar to a h.c.p. structure: A|C|A|C|A|C.... There is an infinite number of possibilities for stacking faults to be introduced in an ordered or disordered fashion, by varying the stacking sequence and the periodicity.

Based on these considerations we can now try to analyse the SAED patterns and to correlate them with the images. Although the SAED pattern in fig. 7 (*b*) exhibits almost perfectly diffuse streaking, microdensitometric measurements show maxima consistent with [010] zone $(Cr, Fe)_2B$ reflections and/or [113] zone $(Fe, Ce)_2B$ reflections. However, these reflections are strongly streaked, indicating a disordered mixture of differently spaced polytypes. It is clear that every lamella of a polytype with a specific spacing (1o, 2o, 3o, etc.) will introduce spots spaced more closely as the periodicity increases, as shown in fig. 9 by FFTs from two such lamellae in the image of fig. 6 (*a*). When small discrete lamellae of differently spaced polytypes are mixed together, their corresponding diffraction spots (each of them additionally streaked) will form an impression of a continuous streak. This is exactly the situation in fig. 7. In spite of the fact that the most repeatable polytype is 2o (see the repeatability histogram in fig. 10), it is present in the form of very thin individual lamellae (five layers maximal thickness), distributed randomly between similarly thin lamellae of other polytypes. These lamellae can be considered as initial nuclei rather than fully developed lamellae. In order to simulate the SAED pattern, various contributions of four basic spacings (1o, 2o, 3o and 4o) were introduced into the calculation, since the intensities of various polytype spots are roughly proportional to their volume fraction in the diffracted volume.

In fig. 6 (*a*) the dominant polytype is also 2o, but it covers even more area than in fig. 7 (*a*) and, even more important, it exists in the form of thick lamellae (the largest being 17 nm thick). Thus the degree of diffuse streaking is substantially lower, as confirmed by densitometric measurements illustrated in fig. 6 (*b*) (compare with fig. 7 (*b*)). This SAED is characteristic of the [0$\bar{1}$3] zone of $(Cr, Fe)_2B$.

Such an interpretation of SAED patterns can explain the (200), (600), etc., diffraction spots in the pattern shown in fig. 3 (*b*), previously identified as [0$\bar{1}$3] SAED of $(Cr, Fe)_2B$. Its analysis is shown in fig. 11. Similar patterns were found by other investigators (Kotani *et al.* 1993, Kesternich and Meertense 1986) and identified as [0$\bar{1}$3] SAED of $(Cr, Fe)_2B$, despite the fact that the (200), (600), etc., reflections should not be present in the actual pattern owing to their low structure factor. However, this could be explained by the superposition of $(2h, 0, 0)$ reflections of the 2o polytypes. Moreover, the additional $(h, 0, 0)$ reflections from the 1o and 3o polytypes will contribute to the observed overall streaking in the zero-order SAED row, while the
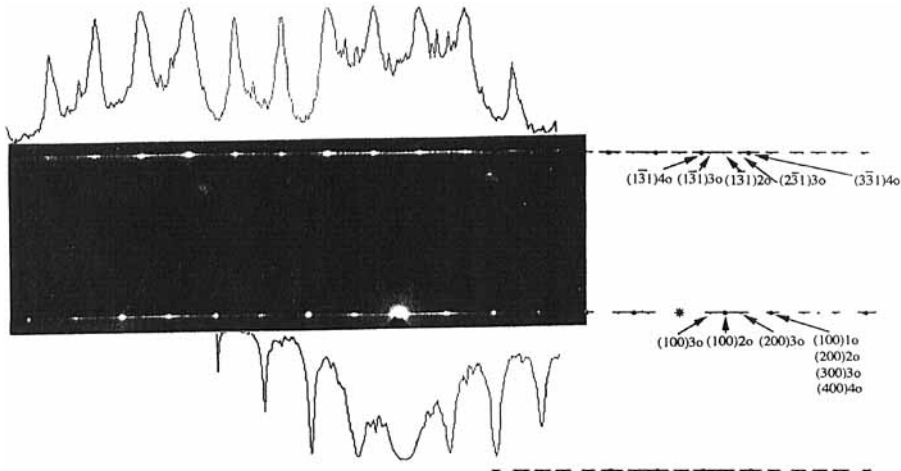
Fig. 9
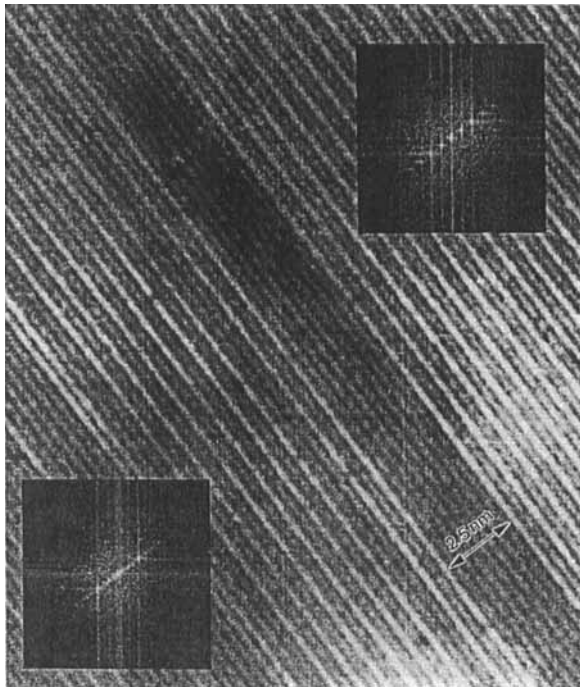
The FTTs obtained from the 1o and the 2o polytype lamellae in fig. 6 (*a*).

Fig. 10
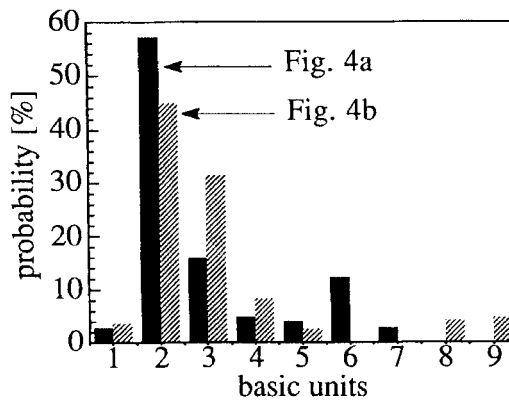
$4a \rightarrow 4(a)$ $4b \rightarrow 4(b)$. The histogram reflecting the probability of variously spaced polytypes. A lamella of one basic unit in width is by definition a stacking fault.

Fig. 11

The magnified $(Cr, Fe)_2B$ [0$\bar{1}$3] SAED pattern shown in fig. 3 (*b*) combined with the densitometric scans of the zero- and the first-order diffraction rows. The computer simulation is given on the right-hand side. The contributions from polytypes of various spacings are indicated.

mixing of various (*hkl*) reflections from the 1o, 2o, 3o and 4o polytypes will contribute to the streaking in the first-order SAED row (see figs. 6 (*b*), 7 (*b*) and 11).

4.2. *The origin of polytypism in* $(Cr, Fe)_2B$

A central question to be asked is why is the $(Cr, Fe)_2B$ phase so strongly faulted and what is the connection, if any, to the discovered polytypism? It is known that phase transformations from f.c.c. to h.c.p. are often accompanied by a profusion of stacking faults and microtwins (Van Torne 1966, Kinsman, Aaronson and Eichen 1971). This is understandable, since the introduction of an intrinsic stacking fault at every third layer in a f.c.c. crystal modifies the stacking sequence to that of h.c.p̄. In this manner the stacking-fault energy can serve as a form of f.c.c. stability criterion. $\beta \rightarrow \alpha$ transformation in SiC is a good example for such a transformation (Ogbuji *et al.* 1981a, Heuer *et al.* 1978). It will be shown that a phase transformation is responsible for the polytypism discovered in $(Cr, Fe)_2B$.

Figure 12 (*a*) presents a detailed analysis of a SAED pattern from the faulted part of a grain shown in fig. 5. Again there is a good match between the experimental and the computer-generated patterns, simulated by varying the contributions from four basic polytypes of $(Cr, Fe)_2B$. It is identified as a [010]-zone $(Cr, Fe)_2B$ pattern. A SAED pattern from the unfaulted half of the crystal matches the [113] zone of $(Fe, Cr)_2B$. The analysis of this pattern is shown in fig. 12 (*b*). The growth front of faults advancing on the {110} atomic planes of $(Fe, Cr)_2B$ and {100} planes of $(Cr, Fe)_2B$ is clearly observed at the boundary between the faulted and the unfaulted portions of the crystal (see fig. 5).

In order to understand why and how the $(Fe, Cr)_2B \rightarrow (Cr, Fe)_2B$ transformation occurs one needs to evaluate the sequence of phase formation in rapidly solidified Fe–C–Cr–B alloys. The large curved particles shown in fig. 1 are the unmelted initial CrB powder particles. Interaction of the powder particles with a molten bath created by the laser beam leads to their partial dissolution as a function of the interaction time

Fig. 12

(a)

(b)
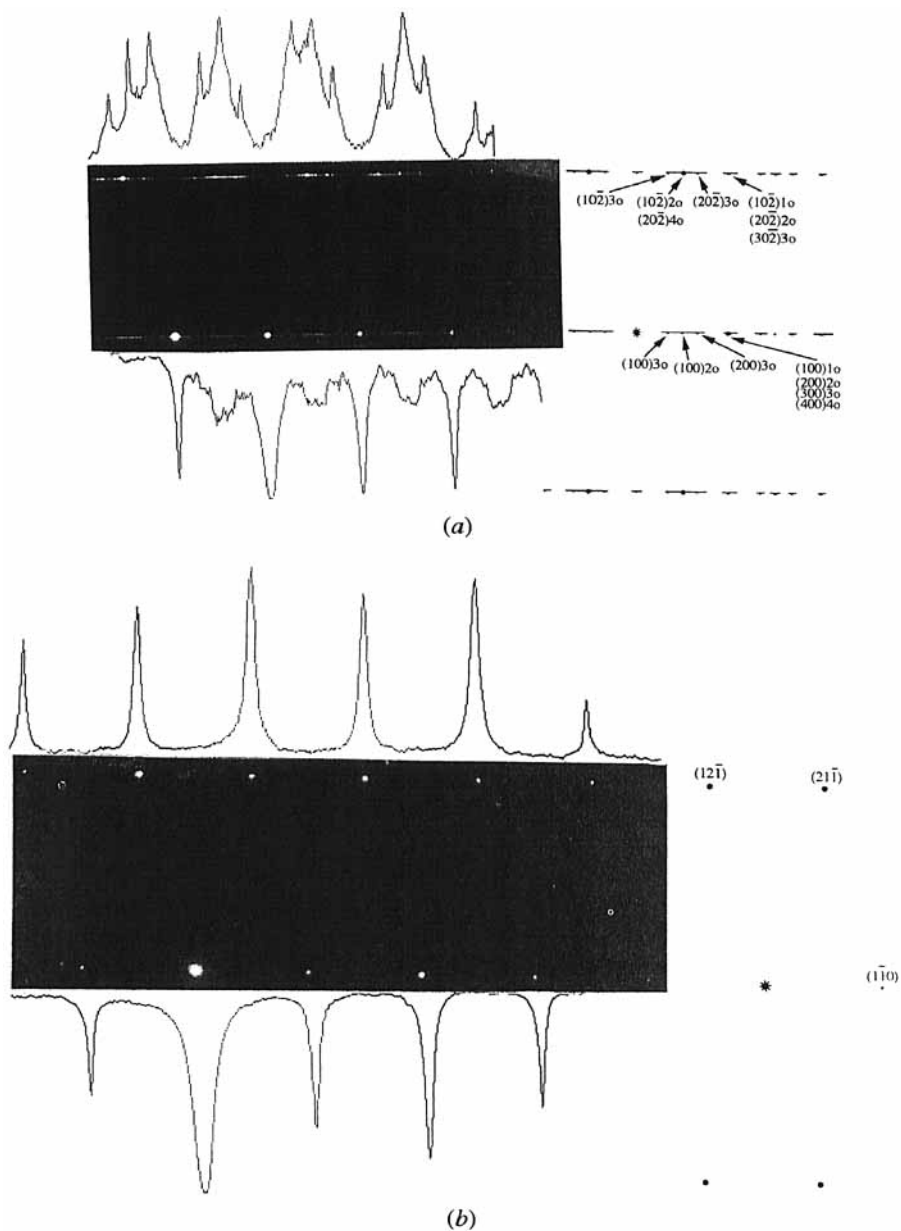
The magnified SAED patterns shown in fig. 5. (*a*) The magnified $(Cr, Fe)_2B$ [010] SAED pattern from the faulted portion of the crystal combined with the densitometric scans of the zero- and the first-order diffraction rows. The computer simulation is given on the right-hand side. The contributions from polytypes of various spacings are indicated. (*b*) The magnified $(Fe, Cr)_2B$ [113] SAED pattern from the unfaulted portion of the crystal combined with the densitometric scans of the zero- and the first-order diffraction rows. The computer simulation is given on the right-hand side. The contributions from polytypes of various spacings are indicated.

between them and the bath. When the powder is fed in at some distance from the laser beam, where the bath begins to cool, only partial dissolution of CrB takes place. On the other hand, a prolonged period of interaction time with the liquid causes the dissolved Cr and B to be distributed over the entire melted layer. The dissolved Cr and B in the vicinity of the undissolved CrB particle react with Fe and C. The columnar grains are probably Fe borides containing Cr, such as $(Fe, Cr)B$ or $(Fe, Cr)_2B$, since their affinity to B is greater than that of Cr (Hack and Chart 1988). Both phases are identified in the XRD patterns. The opposite is correct regarding interaction with carbon. The existence of carbides is hard to confirm using XRD owing to substantial overlaps between the reflections from the various phases. TEM examination failed to reveal carbides, where the region examined by TEM was the region between the columnar grains.

In spite of the absence of known experimental data concerning phase formation in complex Fe–Cr–C–B systems during laser alloying, some analogies from rapidly melt-quenched ribbons can be applied. For example, the estimated cooling rate of melt quenching is $10^5 \, Ks^{-1}$ (Yijian and Jian 1991), which is the same order of magnitude as in laser alloying. The residual liquid between the columns solidifies last and the cooling rate is not sufficiently high to suppress B segregation, which is rejected from the solidifying α-Fe into the regions between the α-Fe grains. As the solidification proceeds, these B-enriched regions form the metastable eutectic structure of α-Fe(Cr) + $(Fe, Cr)_3B$. Metastable $(Fe, Cr)_3B$ having an orthorhombic structure was found in air-quenched ribbons, while tetragonal $(Fe, Cr)_3B$ was found in vacuum melt-quenched ribbons (Yijian and Jian 1991). Both modifications are unstable and tend to disintegrate during annealing, although there is evidence of some stabilization of $(Fe, Cr)_3B$ by carbon (Shafirstien *et al.* 1991). After prolonged annealing (8 h at 800°C), $(Fe, Cr)_3B$ could not be detected in the melt-quenched ribbons. The metastable structure was completely transformed to $(Fe, Cr)_2B$ grains surrounded by grains of α-Fe (Yijian and Jian 1991).

It should be stated here that, although this transformation was not detected in the present experiment, weak lines of the tetragonal $(Fe, Cr)_3B$ were detected by XRD experiments as shown in fig. 2, showing some post-transformation residual $(Fe, Cr)_3B$. Moreover, the microstructure consisting of $(Fe, Cr)_2B$ and $(Cr, Fe)_2B$ surrounded by α-Fe grains (fig. 3 (*a*)) favour a similar transformation. The role of annealing is played by the sequential pass of the laser in the multipass laser scan of the surface. This way every pass anneals the previous one, providing the activation for disintegration of $(Fe, Cr)_3B$. This is actually a very short anneal, contrary to an anneal in melt-quenched samples (Yijian and Jian 1991), which can explain the residual $(Fe, Cr)_3B$ detected by XRD.

However, $(Fe, Cr)_2B$ which is stable in the medium-temperature range (melting point, 1391°C) is less stable in the high-temperature range, relative to $(Cr, Fe)_2B$ (melting point, 1873°C). Therefore, in order to lower the free energy of the system, Cr atoms will leave the α matrix and enter the $(Fe, Cr)_2B$ phase substituting for Fe atoms. It is known that the solubility of Cr in $(Fe, Cr)_2B$ is only 16–20%, in comparison with the solubility of Fe in $(Cr, Fe)_2B$ which is substantially higher (Pradelli and Gianoglio 1976). A $(Cr_{0.9}Fe_{1.1})B_{0.9}$ composition was obtained by vacuum melting of Cr, Fe and B and solidified in a Mn_4B-type structure with parameters very close to Cr_2B (Brown and Beernsten 1964). Therefore the $(Fe, Cr)_2B \rightarrow (Cr, Fe)_2B$ transformation takes place and proceeds by simple atomic substitution and structural adjustment (Yijian and Jian 1991). The $(Fe, Cr)_2B$ structure (*I4/mcm*; tI12, Al_2Cu type) viewed along the [001]

crystallographic direction is shown in fig. 8 (*b*). Both structures are very closely related, being constructed of sheets of tetrahedra of metal atoms with B atoms located in the holes between these sheets, but in $(Fe, Cr)_2B$ there are two systems of sheets of atoms at right angles (Kiessling 1950). This layered configuration is characteristic of known polytypes, especially CdI_2 which consists of tetrahedral I sheets with Cd ions occupying octahedral holes in between. It can be regarded in a different way, as a 'minimal sandwich' of a Cd layer between two I layers, and such 'sandwiches' are linked by weak van der Waals bonds (Verma and Krishna 1966). In our case the 'minimal sandwiches' are A, B, C and D in $(Cr, Fe)_2B$ and A, C in $(Fe, Cr)_2B$. The Cr layers between the B layers, which are weakly bound to each other, give rise to the observed microsyntactic existence of variously spaced polytypes.

As was mentioned earlier, the introduction of stacking faults at every second layer of the $(Cr, Fe)_2B$ structure produces the A|C|A|C|A... stacking sequence, which is the sequence of the $(Fe, Cr)_2B$ structure. This means that $(Fe, Cr)_2B$ can be regarded as faulted $(Cr, Fe)_2B$ (see fig. 8). Only a slight adjustment of B atoms lying on the $\{110\}$ atomic planes of $(Fe, Cr)_2B$ is needed to transform the structure from $(Fe, Cr)_2B$ to $(Cr, Fe)_2B$.

The meaning of the partially faulted grain and the respective SAED patterns can now be interpreted in the framework of this 'fault-induced polytypic transformation' model. As the Cr content in the $(Fe, Cr)_2B$ exceeds the solubility limit, $(Fe, Cr)_2B$ begins to transform into the $(Cr, Fe)_2B$ phase by atomic shifts of boron on $\{110\}$ crystallographic planes. This phase transformation is observed in fig. 5: the lower right-hand part of the image is an untransformed [113]-oriented $(Fe, Cr)_2B$ crystal, progressively becoming an [010]-oriented microsyntactic $(Cr, Fe)_2B$ crystal (upper left-hand region) by producing stacking faults. That is why the SAED pattern of the unfaulted half is unstreaked and does not contain any additional reflections, contrary to the SAED of the already-transformed faulted part of the crystal. The faulting-front step is clearly observed at the transformation boundary (arrowed in fig. 5). The structure is actually a faulted $(Fe, Cr)_2B$ crystal rather than a $(Cr, Fe)_2B$ crystal. However, $(Cr, Fe)_2B$ will heterogeneously nucleate on these faults in order to reach a state of equilibrium. The most stable polytypic configuration appears to be a double-spaced 2o polytype (see the histogram in fig. 10) and this explains the ordered appearance in fig. 6, characterized by fully developed lamellae of one polytype alternating with other grown lamellae. Such an ordered configuration will reduce the streaking of diffraction spots and will produce specific additional (ordering) spots which are characteristic of specific periodicities contributing to the pattern, as can be seen by comparison of the magnified SAED patterns in fig. 6 (*b*) and fig. 12 (*a*).

The mechanism of formation of $(Cr, Fe)_2B$ polytype through the $(Fe, Cr)_2B \rightarrow (Cr, Fe)_2B$ solid state phase transformation resembles that proposed by Ogbuji *et al.* (1981a) for the case of β-SiC $\rightarrow \alpha$-SiC polymorphic transformation. Ogbuji *et al.* proposed that α-SiC nucleates preferentially on β-SiC twin boundaries and on β-SiC stacking faults, since these defects, by their stacking sequence, are incipient α-SiC nuclei. According to their model, stacking faults are formed by partial dislocations generated from incoherent twin boundaries, where the driving force for the motion of such partials is the free-energy reduction accompanying the transformation. Ogbuji *et al.* (1981a) observed partial dislocations at the tips of growing α-SiC lamellae. Thus the observed microsyntaxy is explained by independent heterogeneous nucleation of lamellae at neighbouring twin boundaries and their mutual growth to impingement. The most probable product of such a transformation is an initially heavily faulted basic

polytype. The disordered configuration of faults was observed to take place near the transformation interface, while more ordered configurations existed in the already transformed region, leading to the conclusion that stacking disorders resulting from the transformation anneal-out with time. In the case of $(Fe, Cr)_2B \rightarrow (Cr, Fe)_2B$, growth twins were not commonly observed, and therefore their importance in nucleation is doubtful. On the other hand, the profusion of stacking faults facilitates heterogeneous nucleation. In the present case, faults are most probably formed by partial dislocations generated through thermal stresses during rapid cooling and/or due to non-uniform distribution of elements dissolved in the $(Fe, Cr)_2B$ crystals. The microsyntaxy observed in fig. 7 (a) is probably the result of nucleation of different polytypes on different stacking faults, growing to impingement. Owing to a very densely spaced distribution of faults the resulting lamellae have a limited growth space, which explains their narrow widths (T_1 and T_2 in fig. 7 (a)), in comparison with the relatively well developed lamellae shown in fig. 6 (a). The ordered appearance shown in fig. 6 (a) is believed to form at more final stages of transformation, in agreement with observations of Ogbuji et al. (1981a) and Ogbuji, Mitchell, Heuer and Shinozaki (1981b) in SiC. Furthermore, as was previously mentioned, the surface alloying was made by *scanning* the laser beam over the surface. This way the overlapping laser passes serve as a form of anneal for the already-alloyed regions, which can explain the ordered polytypic configuration shown in fig. 6 (a). The one-dimensionally disordered stacking of undeveloped thin lamellae (or nuclei) shown in fig. 7 (a) may be representative of the regions which solidified last and therefore were not sufficiently annealed in order to become fully ordered.

§ 5. CONCLUSIONS

Surface alloying by laser can improve surface properties, such as hardness and wear resistance, while preserving at the same time the desired bulk properties. In the present work the surface of AISI 1045 steel was laser alloyed with CrB powder. The variety of phases resulting from the laser process, as was revealed by XRD studies, could not be satisfactory explained by SEM examination only. The goal of the current work was to understand the process of phase formation in such a complex rapidly solidified system via detailed TEM examination.

Microstructural studies revealed a profusion of stacking faults present in the grains of the $(Cr, Fe)_2B$ phase. High-magnification phase contrast observations of such grains revealed that they should not be considered simply as heavily faulted, but as ordered and disordered polytypes, differing in the various numbers of structural unit layers stacked in the [100] crystallographic direction. This conclusion was further confirmed by the presence of additional reflections as well as streaking in SAED patterns. Intensely streaked patterns are characteristic of one-dimensionally disordered stacking of various polytypes, while more spotty patterns are evidence of a greater degree of order.

It was also deduced that polytypism in $(Cr, Fe)_2B$ results from the $(Fe, Cr)_2B \rightarrow (Cr, Fe)_2B$ phase transformation. $(Fe, Cr)_2B$ is believed to form during disintegration of the metastable $(Fe, Cr)_3B$ phase, which is in turn formed through the non-equilibrium rapid solidification process of laser alloying. Although this transformation was not actually observed, residual $(Fe, Cr)_3B$ reflections were found by XRD. In addition, eutectic $(Fe, Cr)_3B$ formation followed by subsequent $(Fe, Cr)_3B \rightarrow (Fe, Cr)_2B$ transformation during annealing was established by other researchers in melt-quenched ribbons, which can be regarded as analogous to rapidly

cooled laser-alloyed samples. The role of short annealing is played by subsequent passes of the laser beam during multipass surface scanning.

However, the $(Fe, Cr)_2B$ phase cannot dissolve more than 16–20 wt.% Cr, becoming progressively unstable as the Cr concentration exceeds the solubility limit. On the other hand, the $(Cr, Fe)_2B$ phase can accommodate a much higher concentration of Fe. The same concentrations of Fe and Cr which cause the $(Fe, Cr)_2B$ phase to become unstable can be accommodated in the stable $(Cr, Fe)_2B$ phase. Crystallographic characteristics of both phases are very similar, both being layered structures. $(Fe, Cr)_2B$ can be regarded as a faulted $(Cr, Fe)_2B$ structure. Thus it can be concluded that the $(Fe, Cr)_2B \rightarrow (Cr, Fe)_2B$ phase transformation takes place through the generation of stacking faults in $(Fe, Cr)_2B$, as was observed by TEM analysis, followed by sequential heterogeneous nucleation of $(Cr, Fe)_2B$ on stacking faults. The microsyntactic existence of several $(Cr, Fe)_2B$ polytypes (ordered and disordered) is explained in the framework of this model.

ACKNOWLEDGMENTS

REFERENCES

BAMBERGER, M., BOAZ, M., SHAFIRSTIEN, G., MAISENHALDER, F., and LANGOHR, M., 1991, *Laser Engng.*, **1**, 27.
BROWN, B. E., and BEERSTEN, D. J., 1964, *Acta crystallogr.*, **17**, 448.
CARDUNER, K. R., SHINOZAKI, S. S., ROKOSZ, M. J., PETERS, C. R., and WHALEN, T. J., 1990, *J. Am. Ceram. Soc.*, **73**, 2281.
GARCÍA-BÓRQUEZ, A., and KESTERNICH, W., 1985, *Scripta metall.*, **19**, 57.
GRAF VON MATUSCHKA, A., 1977, *Borienen* (Munich: Carl Hanser).
HACK, K., and CHART, T. G., 1988, Commission of the European Communities Report No. EUR 7820, Part 2.
HEUER, A. H., FRYBURG, G. A., OGBUJI, L. U., MITCHELL, T. E., and SHINOZAKI, S., 1978, *J. Am. Ceram. Soc.*, **61**, 406.
HORNBOGEN, E., and STANIEK, S., 1988, *Z. Metall.*, **79**, 375.
KESTERNICH, W., and MEERTENSE, D., 1986, *Acta metall.*, **34**, 1071.
KIESLING, R., 1950, *Acta chem. scand.*, **4**, 146.
KINSMAN, K. R., AARONSON, H., and EICHEN, E., 1971, *Metall. Trans.*, **2**, 1041.
KOTANI, K., ISHIMASA, T., and OKI, T., 1993, J. Japan Inst. Metals, **57**, 125 (in Japanese).
OGBUJI, L. U., MITCHELL, T. E., and HEUER, A. H., 1981a, *J. Am. Ceram. Soc.*, **64**, 91.
OGBUJI, L. U., MITCHELL, T. E., HEUER, A. H., and SHINOZAKI, S., 1981b, *J. Am. Ceram. Soc.*, **64**, 100.
PRADELLI, G., and GIANOGLIO, G., 1976, *Metall. Ital.*, **68**, 592.
SHAFIRSTIEN, G., BAMBERGER, M., LANGOHR, M., and MAISENHALDER, F., 1991, *Surf. Coat Technol.*, **45**, 417.
SHINOZAKI, S., and KINSMAN, K. R., 1977, *Acta metall.*, **26**, 769.
VAN TORNE, L. I., 1966, *J. appl. Phys.*, **37**, 1849.
VERMA, A. R., and KRISHNA, P., 1966, *Polymorphism and Polytypism in Crystals* (New York: Wiley).
WANG, N., ZHU, F., and HAASEN, P., 1991, *Phil. Mag. Lett.*, **64**, 157.
YIJIAN, L., and JIAN, H., 1991, *J. Mater. Sci.*, **26**, 2833.